Selectivity-Determining Steps in O₂ Reduction Catalyzed by Iron(tetramesitylporphyrin)

**Anna C. Brezny**[†], **Samantha I. Johnson**[‡], **Simone Raugei**[‡], **James M. Mayer**[*,†]

[†]Department of Chemistry, Yale University, New Haven, Connecticut 06520

[‡]Center for Molecular Electrocatalysis, Pacific Northwest National Laboratory, Richland, Washington 99352

Abstract

The oxygen reduction reaction (ORR) is the cathode reaction in fuel cells and its selectivity for water over hydrogen peroxide production is important for these technologies. Iron porphyrin catalysts have long been studied for the ORR, but the origins of their selectivity are not well understood because the selectivity-determining step(s) usually occur after the rate-determining step. We report here the effects of acid concentration, as well as other solution conditions such as of acid pK_a, on the H_2O_2/H_2O selectivity in electrocatalytic ORR by iron tetramesitylporphyrin Fe(TMP) in DMF. The results show that selectivity reflects a kinetic competition in which the dependence on [HX] is one order greater for the production of H_2O than H_2O_2. Based on such experimental results and computational studies, we propose that the selectivity is governed by competition between protonation of the hydroperoxo intermediate, $Fe^{III}(TMP)(OOH)$, to produce water versus dissociation of the HOO^- ligand to yield to H_2O_2. The data rule out a bifurcation based on the regioselectivity of protonation of the hydroperoxide, as suggested in the enzymatic systems. Furthermore, the analysis developed in this study should be generally valuable to the study of selectivity in other multiproton/multielectron electrocatalytic reactions.

SYNOPSIS TOC
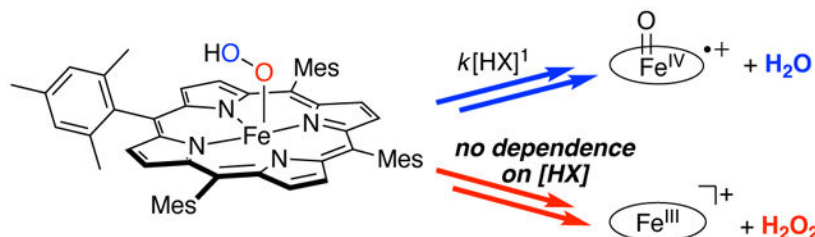
Selective electrocatalysis of multi-electron/multi-proton reactions is key to the development of new technologies for the interconversion of chemical and electrical energies.[1] The oxygen

[*]**Corresponding author**: james.mayer@yale.edu.

The authors declare no competing financial interests.

reduction reaction (ORR) is an important example, being the cathode reaction in fuel cells. Most ORR applications require selective $4e^-/4H^+$ reduction of O_2 to H_2O because the alternative $2e^-/2H^+$ path is less exoergic and the product H_2O_2 is corrosive and hazardous. The ORR selectivities of many soluble and surface-bound iron and cobalt catalysts have been reported,[2–7] and strategies that direct and modulate H^+ and e^- delivery can partially control product formation.[5–6,8–18] Still, the mechanistic origins of selectivity for soluble catalysts are not well understood.

Traditionally, discussions of iron-porphyrin ORR catalysts have used the general mechanism proposed for cytochrome P450 enzymes in which relative rates of proton delivery dictate selectivity (Scheme 1). The branch point is suggested to be the iron-hydroperoxo intermediate Fe^{III}-OOH: protonation at the distal oxygen leads to O-O bond cleavage and production of water, while protonation of the proximal oxygen releases H_2O_2.[3,19] While this scenario is supported by mutagenesis studies,[20–22] the origin of enzymic selectivity is not viewed as a solved problem,[23–26] and is less well understood in molecular systems. Recently, a correlation of selectivity with the electrochemical overpotential (η) has recently been proposed, with less H_2O_2 being formed at higher overpotentials.[27]

This report describes how the selectivity of the ORR by iron tetramesityl-porphyrin Fe(TMP) in N,N-dimethylformamide (DMF) is affected by changes of the catalytic system such as the concentration and pK_a of acid. Our previous mechanistic studies indicated a pathway of pre-equilibrium O_2 binding and rate-determining proton transfer to the iron superoxide complex for ORR catalysis by iron tetraaryl-porphyrins with strong acids in organic media.[30–33] Kinetic studies in this work demonstrate that Fe(TMP) follows the same mechanism, including general acid catalysis.[34] Measurements of the percent H_2O_2 product as a function of the acid pK_a, acid concentration, and other parameters, yield the *relative* rates and rate laws for the selectivity-controlling steps. The results are *not* consistent with (i) the canonical distal vs. proximal protonation origin of ORR selectivity or (ii) a simple correlation between selectivity and η.

Rotating ring-disk voltammetry (RRDV) is the classic method to measure %H_2O_2 produced in the ORR.[7] Catalysis occurs at a central disk, H_2O_2 is oxidized at an outer ring, and the %H_2O_2 is calculated from these currents.[34] This technique was developed for heterogeneous electrocatalysis, but is often used for soluble catalysts. Ideally, the measured selectivity is independent of rotation rate.[27,35–36] Our system did not reach rotation rate independence before the maximum accessible rotation rate, but the relative effects of pK_a and [HX] are consistent across all rotation rates. The conclusions below only depend on the relative effects, not on the absolute values.[34] Furthermore, stoichiometric UV-Vis experiments generating H_2O and H_2O_2 from the independently generated iron-peroxo complex support the same conclusions as the RRDV results.[34] Typical RRDV conditions had 0.2 mM of the iron catalyst ([Fe(TMP)][OTf]), 100 mM [NBu$_4$][PF$_6$], 1 atm (3.1 mM) O_2, and 10–100 mM acid in DMF. All experiments were performed in buffered acid to fix the overpotential.[37,38] The reported selectivities are from measurements at the fastest obtainable rotation rate (3000 RPM).

The pK_a of the buffered acid was varied from -1.1 to 6 using protonated DMF triflate ([H-DMF]OTf, -1.1), *p*-toluenesulfonic acid (*p*-TsOH, 2.6), sulfuric acid (H_2SO_4, 3.1), and trifluoracetic acid (TFA, 6.0).[39,40] A very shallow correlation between pK_a and selectivity was observed: as the strength of the acid (K_a) decreases by 10^7, only slightly more H_2O_2 is produced, from 0.9 to 20% (Figure 1A). In contrast, the selectivity shows a steep dependence on the *concentration* of buffered acid. Decreasing the concentration of 1:1 HA:A$^-$ tenfold led to roughly ten times more H_2O_2 (Figure 1B, blue circles).

Varying the overpotential by changing the acid pK_a gives the same selectivity trend observed by Nocera and coworkers for dicobalt and Fe(porphyrin) catalysts (Figure 2A).[27,41] However, this thermodynamic relationship cannot be complete. Changes in the concentration of 1:1 buffer do not change the overpotential, because only the ratio of [HA]/[A$^-$] appears in the Nernst equation (Figure 2B, blue circles).[37] Therefore, the steep selectivity dependence on buffer concentration *reflects the kinetics of the bifurcation and not the thermodynamics.* This result contrasts with the simple overpotential-selectivity relationship previously proposed.[27]

We varied η based on the Nernst equation dependence on [HA]/[A$^-$] by independently varying [*p*-TsOH] and [*p*-TsONa]. Altering [*p*-TsOH] while holding [*p*-TsONa] constant changes η, but led to the same selectivities as when the 1:1 buffer concentration was varied (Figures 1B and 2B, red diamonds). In contrast, there was no change in selectivity observed when [*p*-TsOH] was held constant and [*p*-TsONa] was varied, which also impacts η (Figure 2B green triangles). These observations again show that the %H_2O_2 produced is not determined by overpotential, but instead by [*p*-TsOH].

The observed acid dependence rules out, at least for this system, the commonly proposed origin of the H_2O/H_2O_2 selectivity. The traditional mechanism in Scheme 1, involving protonation either at the proximal or the distal oxygen, requires a first order dependence on [HX] for *both* pathways from the Fe(TMP)(OOH) intermediate. An increase in [HX] should increase the rates of H_2O and H_2O_2 formation *equally* and therefore lead to no change in selectivity. The data in Figures 1&2 therefore require a different mechanism.

Our analysis of the effects of protons on the H_2O/H_2O_2 selectivity uses the generic kinetic model in Scheme 2, starting from the Fe(TMP)(OOH) intermediate.[42] The step(s) to generate water involve some dependence on the acid (*a*HX) and therefore has the rate law in eq 1. Analogously, the rate of H_2O_2 formation involves *b*HX (eq 2). Because these steps occur after the turnover-determining step, the k_{H_2O} and $k_{H_2O_2}$ and dependencies on [HX] cannot be determined kinetically. However, the ratio of these equations gives an expression for the selectivity, [H_2O_2]/[H_2O] (eq 3). Equation 3 can be manipulated to solve for the difference in reaction orders in acid, b–a (eq 4).[34] Plotting our data according to eq 4 (Figure 3A) gives a straight line with slope b-a=-1. Thus the H_2O_2 pathway has a kinetic dependence on [HX] (rate$\propto$[HX]^b) that is one order lower than the H_2O pathway (rate$\propto$[HX]$^{b+1}$). This result contrasts with the lack of selectivity change reported for dicobalt ORR catalysts upon changing [HX],[27] so the two systems must have different mechanisms.

$$\frac{d[\text{H}_2\text{O}]}{d\text{t}} = 2k_{H_2O}[\text{FeOOH}][\text{HX}]^a \tag{1}$$

$$\frac{d[\text{H}_2\text{O}_2]}{d\text{t}} = k_{H_2O_2}[\text{FeOOH}][\text{HX}]^b \tag{2}$$

$$\frac{d[\text{H}_2\text{O}_2]}{d[\text{H}_2\text{O}]} = \frac{k_{H_2O_2}}{2k_{H_2O}}[\text{HX}]^{b-a} = \frac{[\text{H}_2\text{O}_2]}{[\text{H}_2\text{O}]} \tag{3}$$

$$\frac{\partial \log\left(\frac{[\text{H}_2\text{O}_2]}{(\text{H}_2\text{O}]}\right)}{\partial \log\left([\text{H}^+]\right)} = b - a \tag{4}$$

Quantum chemical analysis based on density functional theory (DFT) optimizations and hybrid DFT/molecular mechanics free energy simulations provided insight into the mechanisms that give rise to these dependencies on [HX] for the two pathways.[34] Calculations strongly indicate that formation of H_2O is first order in acid (a=1), while formation of H_2O_2 is zero order in acid (b=0), consistent with the experimental constraint b–a=−1. Protonation of the distal oxygen by H-DMF$^+$ in DMF leads to a very exoergic H_2O release ($G°$=−48.0 kcal mol^{-1}) via a short-lived [Fe(TMP)(OOH$_2$)]$^+$ intermediate ($G°$= −5.7 kcal mol^{-1}). The kinetic instability of this cationic intermediate rules out H_2O formation via a mechanism that is second order in acid, and implies that only one proton is required to produce H_2O (Scheme 3, bottom; as in Scheme 1). This conclusion suggests that H_2O_2 formation proceeds via the unimolecular dissociation of HOO$^-$, which is quickly protonated by the exogenous acid in solution (Scheme 3, top). Additional computational analysis, including ca. 20 mM H_2O, revealed that the unimolecular dissociation of HOO$^-$ ($G^{\ddagger} = 10.5$ kcal mol^{-1}) is kinetically considerably more favorable than the release of H_2O_2 by protonation of the proximal oxygen, which is highly hindered sterically ($G^{\ddagger}$=29.1 kcal mol^{-1}). Water is present in our dried DMF and is the major product of catalysis; we conservatively estimate ca. 20 mM H_2O near the electrode.[34] Our simulations showed that water facilitates the heterolytic breaking of the Fe-OOH bond over the homolytic bond breaking ($G^{\ddagger}$=12.5kcal mol^{-1}) by solvating HOO$^-$, resulting in a very exoergic release of HOO$^-$ (G=−46.5 kcal mol^{-1} in 0.02M water/DMF).

The shallow dependence of selectivity on pK_a (Figures 1A and 3B) is consistent with this mechanism. With the conclusion that only the H_2O pathway is dependent on the acid concentration, changing the pK_a only influences k_{H_2O}. The change in a proton transfer rate constant with a change in pK_a is given by the Brønsted equation, eq 5.[43] The value of a can indicate the asymmetry of the proton transfer reaction, with a=0.5 suggesting a symmetrical process. Combining the Brønsted equation and eq 3 above, with a=1, b=0, gives eq 6.[34] Plotting the data according to eq 6 (Figure 3B) gives $\alpha_{H_2O} = 0.2$. This is consistent with distal protonation of Fe(TMP)(OOH) because this exoergic step would typically have

$\alpha_{H_2O} < 0.5$ based on Hammond's postulate and because protonations of related superoxide intermediates have been found to have a small based on Hammond's postulate and because α's.[44]

$$\Delta\log(k_{\text{HA}}) = -\alpha\Delta pK_a \tag{5}$$

$$\frac{\partial\log\left(\frac{[H_2O_2]}{[H_2O]}\right)}{\partial pK_a} = \alpha_{H_2O} \tag{6}$$

Several additional mechanistic experiments are consistent with our proposal that HOO⁻ dissociates to generate H_2O_2. First, the selectivity of ORR using an extremely bulky proton donor (2,6-di-tertbutyl pyridinium triflate, pKa ~ 1)[34,40,45–47] gave more H_2O_2 than expected based on the pK_a trend in Figure 1A (12% versus ~3% H_2O_2). This is consistent with our proposal because the very bulky acid (with a bulky porphyrin) slows only the rate of water formation, not dissociation of OOH⁻. If proximal protonation were required to form H_2O_2, the very bulky acid should give *less* H_2O_2 than a sterically accessible acid. Second, the ORR in acetonitrile is an order of magnitude more selective for water than the reaction under identical conditions in DMF. This, too, is consistent with a mechanism in which H_2O_2 comes from HOO⁻ dissociation, because this pathway should be suppressed in solvents that are less effective at solubilizing anions, such as MeCN compared to DMF.[48,49] Alternative mechanisms involving pre-equilibria or different orders in acid were considered but are inconsistent with the experimental data.[34]

In summary, exploring the effect of reaction conditions on selectivity enabled the study of steps that are kinetically invisible (that are after the rate-determining-step). The analysis described here demonstrates that the rate law for forming water from the Fe(TMP)(OOH) intermediate requires one more HX compared to the H_2O_2 rate expression. This kind of fundamental understanding of the origins of selectivity in iron porphyrin-catalyzed oxygen reduction has not previously been available. Our results in DMF contrast with the traditional mechanism for H_2O_2 production by heme enzymes in which regioselectivity of protonation determines product selectivity.[28] The conclusions here may be relevant to new oxygen reduction catalysis in new energy technologies, to help optimize selectivity as well as overpotential and TOF. More generally, the approach developed here will be broadly applicable to unravelling the origins of selectivities in multi-electron, multi-proton catalytic reactions.

Supplementary Material

Refer to Web version on PubMed Central for supplementary material.

ACKNOWLEDGMENT

the Cascade supercomputer at EMSL, a national scientific user facility sponsored by the DOE's Office of Biological and Environmental Research and located at PNNL.

REFERENCES

(1). Winter M; Brodd RJ What Are Batteries, Fuel Cells, and Supercapacitors? Chem. Rev 2004, 104, 4245–4270. [PubMed: 15669155]

(2). Pegis ML; Wise CF; Martin DJ; Mayer JM Oxygen Reduction by Homogeneous Molecular Catalysts and Electrocatalysts. Chem. Rev 2018, 118, 2340–2391. [PubMed: 29406708]

(3). Zhang W; Lai W; Cao R Energy-Related Small Molecule Activation Reactions: Oxygen Reduction and Hydrogen and Oxygen Evolution Reactions Catalyzed by Porphyrin- and Corrole-Based Systems. Chem. Rev 2017, 117, 3717–3797. [PubMed: 28222601]

(4). Gewirth AA; Varnell JA; DiAscro AM Nonprecious Metal Catalysts for Oxygen Reduction in Heterogeneous Aqueous Systems. Chem. Rev 2018, 118, 2313–2339. [PubMed: 29384375]

(5). Chatterjee S; Sengupta K; Mondal B; Dey S; Dey A Factors Determining the Rate and Selectivity of $4e^-/4H^+$ Electrocatalytic Reduction of Dioxygen by Iron Porphyrin Complexes. Acc. Chem. Res 2017, 50, 1744–1753. [PubMed: 28686419]

(6). Wang YH; Schneider PE; Goldsmith ZK; Mondal B; Hammes-Schiffer S; Stahl SS Bronsted Acid Scaling Relationships Enable Control Over Product Selectivity from O_2 Reduction with a Mononuclear Cobalt Porphyrin Catalyst. ACS Cent. Sci 2019, 5, 1024–1034. [PubMed: 31263762]

(7). Collman JP; Boulatov R; Sunderland CJ; Fu L Functional Analogues of Cytochrome c Oxidase, Myoglobin, and Hemoglobin. Chem. Rev 2004, 104, 561–588. [PubMed: 14871135]

(8). Dey S; Mondal B; Chatterjee S; Rana A; Amanullah S; Dey A Molecular electrocatalysts for the oxygen reduction reaction. Nat. Rev. Chem 2017, 1, 0098.

(9). Collman JP Synthetic models for the oxygen-binding hemoproteins. Acc. Chem. Res 1977, 10, 265–272.

(10). Rosenthal J; Nocera DG Role of Proton-Coupled Electron Transfer in O–O Bond Activation. Acc. Chem. Res 2007, 40, 543–553. [PubMed: 17595052]

(11). McGuire R Jr; Dogutan DK; Teets TS; Suntivich J; Shao-Horn Y; Nocera DG Oxygen reduction reactivity of cobalt(II) hangman porphyrins. Chem. Sci 2010, 1, 411–414.

(12). Dogutan DK; Stoian SA; McGuire R; Schwalbe M; Teets TS; Nocera DG Hangman Corroles: Efficient Synthesis and Oxygen Reaction Chemistry. J. Am. Chem. Soc 2011, 133, 131–140. [PubMed: 21142043]

(13). Halime Z; Kotani H; Li Y; Fukuzumi S; Karlin KD Homogeneous catalytic O_2 reduction to water by a cytochrome c oxidase model with trapping of intermediates and mechanistic insights. Proc. Natl. Acad. Sci 2011, 108, 13990–13994. [PubMed: 21808032]

(14). Matson BD; Carver CT; Von Ruden A; Yang JY; Raugei S; Mayer JM Distant protonated pyridine groups in water-soluble iron porphyrin electrocatalysts promote selective oxygen reduction to water. Chem. Commun 2012, 48, 11100–11102.

(15). Bhunia S; Rana A; Roy P; Martin DJ; Pegis ML; Roy B; Dey A Rational Design of Mononuclear Iron Porphyrins for Facile and Selective $4e^-/4H^+$ O_2 Reduction: Activation of O-O Bond by 2nd Sphere Hydrogen Bonding. J. Am. Chem. Soc 2018, 140, 9444–9457. [PubMed: 29975839]

(16). Mukherjee S; Mukherjee M; Mukherjee A; Bhagi-Damodaran A; Lu Y; Dey A O_2 Reduction by Biosynthetic Models of Cytochrome c Oxidase: Insights into Role of Proton Transfer Residues from Perturbed Active Sites Models of CcO. ACS Catal. 2018, 8, 8915–8924.

(17). Singha A; Mittra K; Dey A Effect of hydrogen bonding on innocent and non-innocent axial ligands bound to iron porphyrins. Dalton Trans. 2019, 48, 7179–7186. [PubMed: 30564827]

(18). Wang L; Gennari M; Cantu Reinhard FG; Gutierrez J; Morozan A; Philouze C; Demeshko S; Artero V; Meyer F; de Visser SP; Duboc C A Non-Heme Diiron Complex for (Electro)catalytic Reduction of Dioxygen: Tuning the Selectivity through Electron Delivery. J. Am. Chem. Soc 2019, 141, 8244–8253. [PubMed: 31026148]

(19). Meunier B; de Visser SP; Shaik S Mechanism of Oxidation Reactions Catalyzed by Cytochrome P450 Enzymes. Chem. Rev 2004, 104, 3947–3980. [PubMed: 15352783]

(20). Martinis SA; Atkins WM; Stayton PS; Sligar SG A conserved residue of cytochrome P-450 is involved in heme-oxygen stability and activation. J. Am. Chem. Soc 1989, 111, 9252–9253.

(21). Imai M; Shimada H; Watanabe Y; Matsushima-Hibiya Y; Makino R; Koga H; Horiuchi T; Ishimura Y Uncoupling of the cytochrome P-450cam monooxygenase reaction by a single mutation, threonine-252 to alanine or valine: possible role of the hydroxy amino acid in oxygen activation. Proc. Natl. Acad. Sci 1989, 86, 7823–7827. [PubMed: 2510153]

(22). Davydov R; Makris TM; Kofman V; Werst DE; Sligar SG; Hoffman BM Hydroxylation of Camphor by Reduced Oxy-Cytochrome P450cam: Mechanistic Implications of EPR and ENDOR Studies of Catalytic Intermediates in Native and Mutant Enzymes. J. Am. Chem. Soc 2001, 123, 1403–1415. [PubMed: 11456714]

(23). Guallar V; Friesner RA Cytochrome P450CAM Enzymatic Catalysis Cycle: A Quantum Mechanics/Molecular Mechanics Study. J. Am. Chem. Soc 2004, 126, 8501–8508. [PubMed: 15238007]

(24). Nagano S; Poulos TL Crystallographic Study on the Dioxygen Complex of Wild-type and Mutant Cytochrome P450cam: Implications For The Dioxygen Activation Mechanism. J. Biol. Chem 2005, 280, 31659–31663. [PubMed: 15994329]

(25). Makris TM; von Koenig K; Schlichting I; Sligar SG Alteration of P450 Distal Pocket Solvent Leads to Impaired Proton Delivery and Changes in Heme Geometry. Biochemistry 2007, 46, 14129–14140. [PubMed: 18001135]

(26). Poulos TL Heme enzyme structure and function. Chem. Rev 2014, 114, 3919–3962. [PubMed: 24400737]

(27). Passard G; Ullman AM; Brodsky CN; Nocera DG Oxygen Reduction Catalysis at a Dicobalt Center: The Relationship of Faradaic Efficiency to Overpotential. J. Am. Chem. Soc 2016, 138, 2925–2928. [PubMed: 26876226]

(28). Makris TM; Denisov I; Schlichting I; Sligar SG In Cytochrome P450: Structure, Mechanism, and Biochemistry; Ortiz de Montellano PR, Ed.; Springer US: Boston, MA, 2005, p 149–182.

(29). Mak PJ; Denisov IG Spectroscopic studies of the cytochrome P450 reaction mechanisms. Biochim. Biophys. Acta 2018, 1866, 178–204.

(30). Pegis ML; Martin DJ; Wise CF; Brezny AC; Johnson SI; Johnson LE; Kumar N; Raugei S; Mayer JM Mechanism of Catalytic O_2 Reduction by Iron Tetraphenylporphyrin. J. Am. Chem. Soc 2019, 141, 8315–8326. [PubMed: 31042028]

(31). Pegis ML; McKeown BA; Kumar N; Lang K; Wasylenko DJ; Zhang XP; Raugei S; Mayer JM Homogenous Electrocatalytic Oxygen Reduction Rates Correlate with Reaction Overpotential in Acidic Organic Solutions. ACS Cent. Sci 2016, 2, 850–856. [PubMed: 27924314]

(32). Pegis ML; Wise CF; Koronkiewicz B; Mayer JM Identifying and Breaking Scaling Relations in Molecular Catalysis of Electrochemical Reactions. J. Am. Chem. Soc 2017, 139, 11000–11003. [PubMed: 28724290]

(33). Wasylenko DJ; Rodríguez C; Pegis ML; Mayer JM Direct Comparison of Electrochemical and Spectrochemical Kinetics for Catalytic Oxygen Reduction. J. Am. Chem. Soc 2014, 136, 12544–12547. [PubMed: 25137524]

(34). See Supporting Information (SI) for details.

(35). Rigsby ML; Wasylenko DJ; Pegis ML; Mayer JM Medium effects are as important as catalyst design for selectivity in electrocatalytic oxygen reduction by iron-porphyrin complexes. J. Am. Chem. Soc 2015, 137, 4296–4299. [PubMed: 25798713]

(36). Bettelheim A; Kuwana T Rotating-ring-disk analysis of iron tetra(N-methylpyridyl)porphyrin in electrocatalysis of oxygen. Anal. Chem 1979, 51, 2257–2260.

(37). Appel AM; Helm ML Determining the Overpotential for a Molecular Electrocatalyst. ACS Catal. 2014, 4, 630–633.

(38). Pegis ML; Roberts JA; Wasylenko DJ; Mader EA; Appel AM; Mayer JM Standard Reduction Potentials for Oxygen and Carbon Dioxide Couples in Acetonitrile and N,NDimethylformamide. Inorg. Chem 2015, 54, 11883–11888. [PubMed: 26640971]

(39). The pKa of HDMF+ in DMF is typically taken as 0 (Typically, Kc = [HDMF+][DMF]/([HDMF+][DMF]) = 1). When comparing to other acids, it is important to take into account the

concentration of DMF (13 M). Ka = Kc [DMF] = [HDMF+][DMF]/[HDMF+] = [DMF]. pKa = − log(Ka) = −log(13) = −1.1.

(40). For pKas of acids in non-aqueous solvents, see: Izutsu K Electrochemistry in Nonaqueous Solutions; Wiley-VCH Verlag GmbH & Co.: Weinheim, 2002.

(41). We prefer to plot $\log(\%H_2O_2)$ rather than $\%H_2O_2$ because linear free energy relations (LFERs) correlate logarithms of rate constants and concentrations..

(42). See SI for discussion of the unobserved FeIII(TMP)(OOH) hydroperoxo species being the likely bifurcation point. Rate-determining protonation of the superoxide30 should be rapidly followed by highly exergonic reduction of [FeIII(TMP)(•OOH)]+ to FeIII(TMP)(OOH).

(43). Brönsted JN; Pedersen K The catalytic decomposition of nitramide and its physico-chemical applications. Z. Phys. Chem 1925, 108, 185.

(44). α = 0.16(1) for Fe(TMP) (see SI for more details) and ~0.3 for other Fe(tetraarylporphyrin) catalysts (Ref 32 and 33).

(45). Poliak P The DFT calculations of pKa values of the cationic acids of aniline and pyridine derivatives in common solvents. Acta Chimica Slovaca 2014, 7, 25–30.

(46). Benoit RL; Fréchette M; Lefebvre D 2,6-Di-tertbutylpyridine: an unusually weak base in dimethylsulfoxide. Can. J. Chem 1988, 66, 1159–1162.

(47). Kostikov RR; Francisco S-S; Garranzo M; Murcia MC 2,6-Di-t-butylpyridine. In Encyclopedia of Reagents for Organic Synthesis; Paquette LA, Ed.; John Wiley & Sons, Ltd.: Hoboken, NJ, 2010. doi:10.1002/047084289X.rd068.pub2

(48). Catalan J On the π^* Solvent Scale. The Journal of Organic Chemistry 1995, 60, 8315–8317.

(49). Anslyn EV; Dougherty DA In Modern Physical Organic Chemistry; University Science Books: Sausalito, California, 2006, p 145–205.
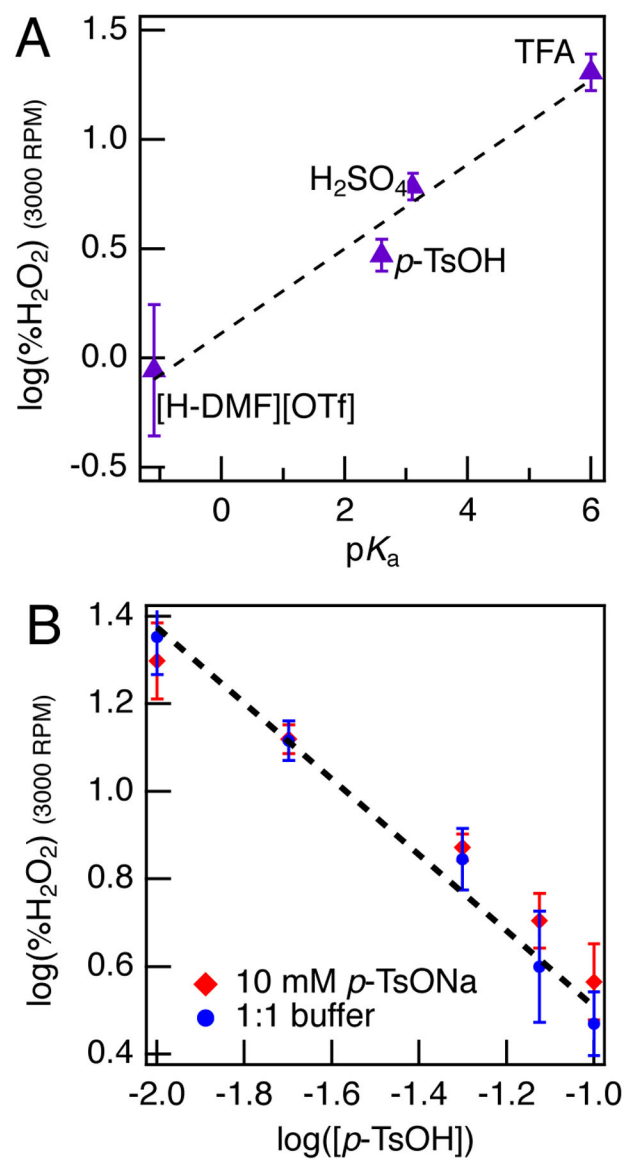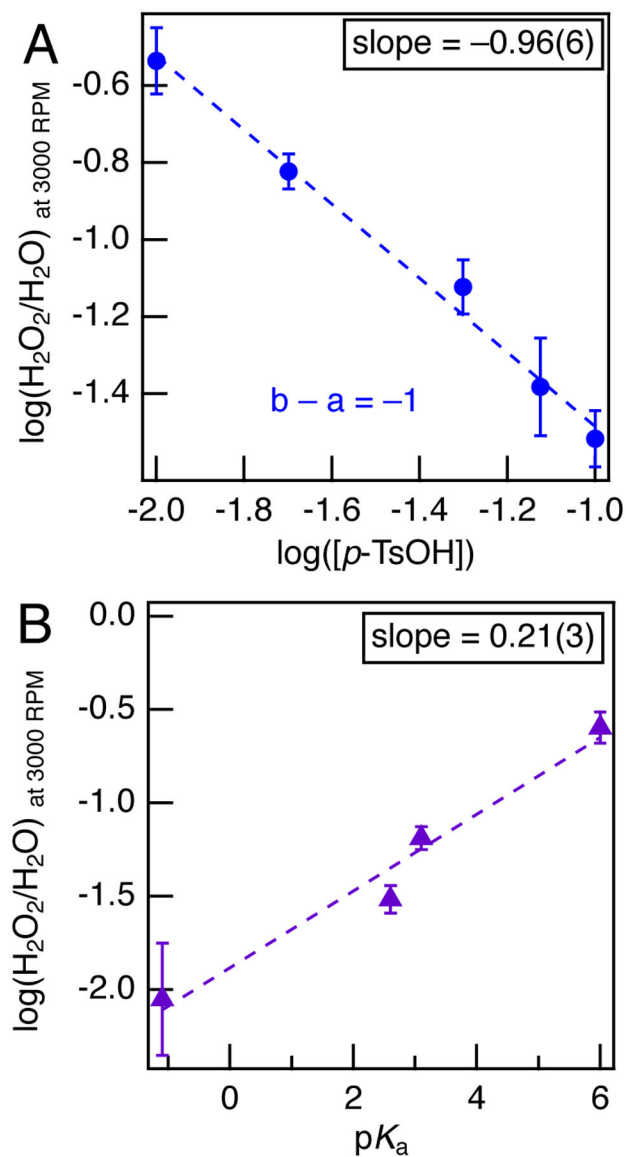
Figure 1.
A: Dependence of $\log(\%H_2O_2)$ on pK_a of the exogenous acid (standard conditions, 100 mM buffered acid). **B**: Correlation between $\log(\%H_2O_2)$ and $\log([p\text{-}TsOH])$ under standard conditions, with either a 1:1 p-TsOH:p-TsONa buffer (blue circles) or with constant $[p\text{-}TsONa] = 0.01$ M (red diamonds).
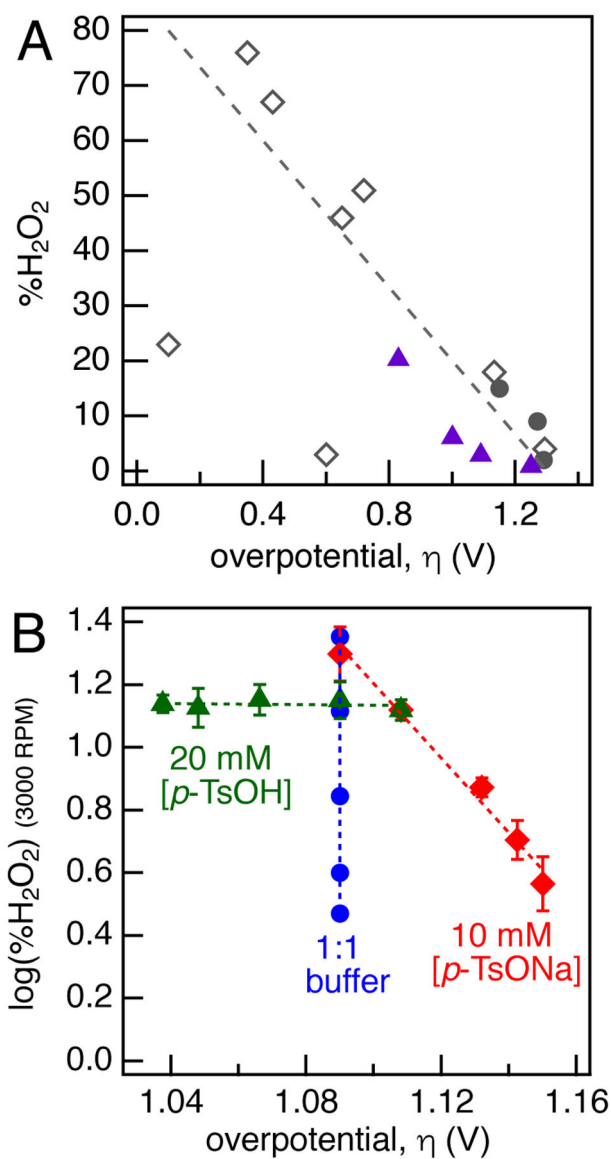
Figure 2.
A: Reported correlation between $\%H_2O_2$ and overpotential, adapted from ref. 27 (dicobalt catalysts, $\diamondsuit$; prior Fe(porphyrin) catalysts, $\bullet$) with the addition of Fe(TMP) results from this work (violet triangles). **B**: $\log(\%H_2O_2)$ versus overpotential under standard conditions with: 0.01–0.1 M 1:1 buffered p-TsOH:p-TsONa (blue circles); 0.01–0.1 M p-TsOH buffered with 0.01 M p-TsONa (red diamonds); 0.02 M p-TsOH buffered with 0.01–0.1 M p-TsONa (green triangles).

Figure 3.
Plots of $\log([H_2O_2]/[H_2O])$ **A**: versus $\log([p\text{-TsOH}])$; the slope is the difference in the kinetic orders in [HX] for H_2O_2-vs.-H_2O formation. **B**: versus pK_a; the slope is the difference in Brønsted a's for H_2O and H_2O_2 production.
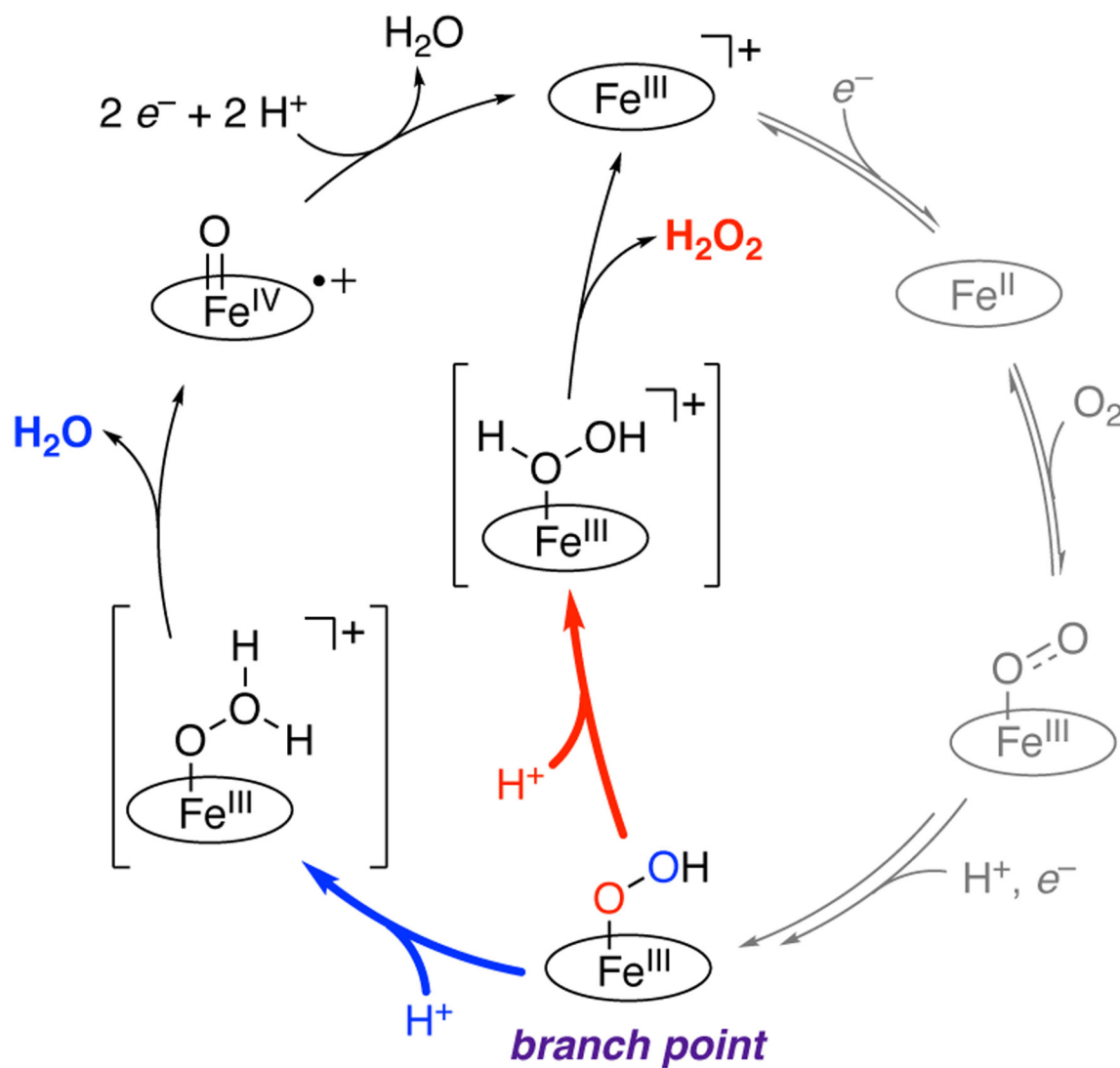
Scheme 1.
Canonical mechanism[2–5,20–26,28,29] for H_2O_2 and H_2O selectivity in cytochrome P450 and Fe(porphyrin) systems. Expanded from ref. 30.
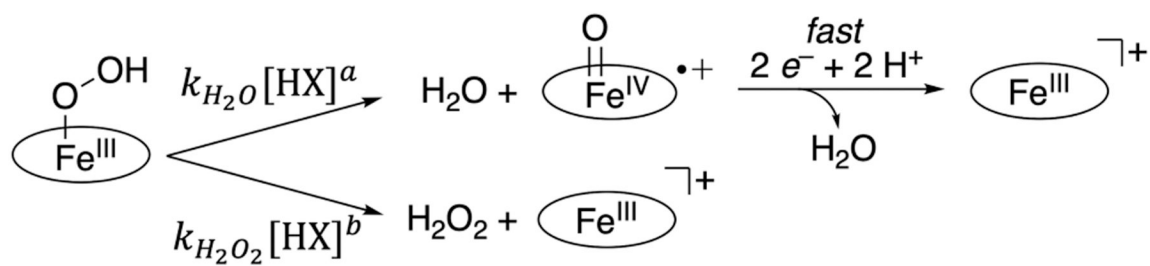
Scheme 2.
Kinetic analysis of the bifurcating pathways from the Fe(TMP)(OOH) intermediate.
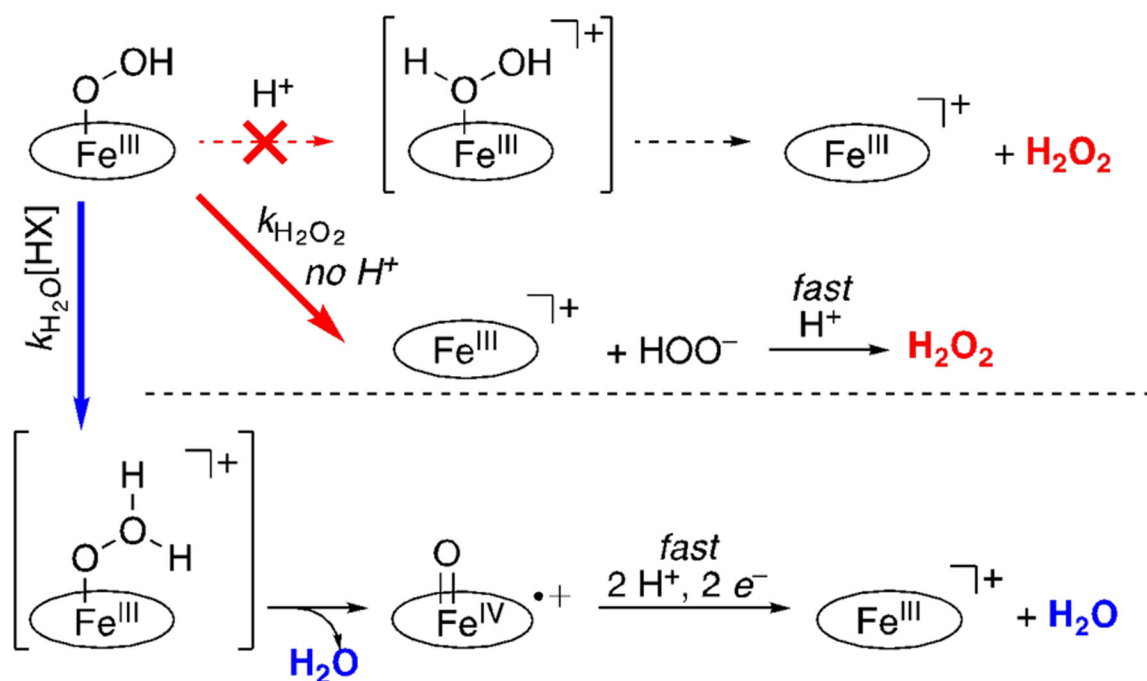
Scheme 3.
Proposed mechanism for the bifurcation in the ORR catalyzed by Fe(TMP).